

Application of a variable filter for presampled modulation transfer function analysis with the edge method

メタデータ	言語: eng 出版者: 公開日: 2017-10-03 キーワード (Ja): キーワード (En): 作成者: メールアドレス: 所属:
URL	http://hdl.handle.net/2297/43456

Application of a variable filter for presampled modulation transfer function analysis
with the edge method

Authors: Ryo Higashide · Katsuhiko Ichikawa · Hiroshi Kunitomo · Kazuya Ohashi

Corresponding author: Ryo Higashide

R. Higashide

Graduate School of Medical Science, Kanazawa University, 5-11-80 Kodatsuno,

Kanazawa, Ishikawa 920-0942, Japan

e-mail: raryo@med.nagoya-cu.ac.jp

K. Ichikawa

Institute of Medical, Pharmaceutical and Health Sciences, Kanazawa University,

5-11-80 Kodatsuno, Kanazawa, Ishikawa 920-0942, Japan

R. Higashide · H. Kunitomo · K. Ohashi

Department of Radiology, Nagoya City University Hospital, 1 Kawasumi, Mizuho-cho,

Mizuho-ku, Nagoya, Aichi 467-0001, Japan

Abstract

We devised a new noise filtering method to reduce the noise in the line spread function (LSF) for presampled modulation transfer function (MTF) analysis with the edge method. A filter was designed to reduce noise effectively by using a position-dependent filter controlled by the boundary frequency b for low-pass filtering, which is calculated by $1/2d$ (d : distance from the LSF center). In this filtering process, strong filters with very low b can be applied to regions distant from the LSF center, and the region near the LSF center can be maintained simultaneously by a correspondingly high b . Presampled MTF accuracies derived by use of the proposed method and an edge spread function (ESF)-fitting method were compared by use of simulated ESFs with and without noise, resembling a computed radiography (CR) and an indirect-type flat panel detector (FPD), respectively. In addition, the edge images of clinical CR, indirect-type FPD and direct-type FPD systems were also examined. For simulated ESF without noise, calculated MTFs of the variable filtering method agreed precisely with the true MTFs. The excellent noise-reduction ability of the variable filter was demonstrated for all simulated noisy ESFs and those of three clinical systems. Although the ESF-fitting method only provided excellent noise reduction for the CR-like simulated ESF with noise, its noise elimination performance could not be demonstrated due to the lesser robustness of the fitting.

Keywords: Presampled modulation transfer function (MTF) · Edge method · Digital radiography · Variable filter · Noise reduction technique

1 Introduction

The presampled modulation transfer function (MTF), for which various measurement methods have been proposed [1-9], is useful for assessment of the resolution properties of digital radiography (DR) systems. Among the proposed methods, the edge method was recommended in the International Electrotechnical Commission (IEC) standard, IEC 62220-1 [5, 6] and has been widely used. In the edge method, a metal plate (tungsten plates were recommended in the IEC standards) with precisely polished edges is placed on the detector surfaces, slightly slanted with respect to the pixel array, and imaged. This method is very susceptible to noise within the image, which is enhanced by the differentiation process used for converting the edge profile (edge spread function: ESF) to a line spread function (LSF) [8, 10-13]. However, as compared with the slit method, the edge method can provide more accurate MTFs at low spatial frequencies [8, 10, 12, 14], and it is better able to obtain edge images because of its lower sensitivity to X-ray beam alignment errors [8]. Samei et al. reduced the ESF noise by using a binning technique during the process of reprojection from a two-dimensional edge image to ESF, and subsequently used a Gaussian-weighted moving polynomial fit for the ESF obtained [8]. Boone and Seibert also eliminated noise enhancement by an ESF-fitting technique using a parametric equation [15].

For presampled MTF measurements of DR systems with glare, long-range ESFs

exceeding 8 cm are required for correct evaluation of a low frequency drop (LFD) in the MTF, which is caused by glare [12, 16, 17]. In general, the enhanced LSF noise generated in the edge method is noticeable in the LSF tail on the direct exposure (high exposure) side, and the noise therefore causes remarkable errors with fluctuating MTF values over the entire frequency range.

As the noise-reduction performance of the above-mentioned binning and polynomial fit techniques was insufficient, ESF or MTF averaging techniques have been desired [7]. However, for computed radiography (CR) systems, the ESF averaging technique requires attention in terms of the misregistrations between multiple obtained images, and these averaging techniques are time consuming because of repeated image acquisitions and MTF analyses. Therefore, it appears that the ESF-fitting technique would be most effective if the fitting were robust for various types of DR systems. However, in the study of Boone and Seibert, the ESF fitting method was validated using only one digital mammography system with charge couple device (CCD) combined with an intensifying screen, and the robustness of the method has not yet been confirmed using various types of detectors.

In this paper, we propose a newly developed variable filter that can reduce LSF noise by using a position-dependent low-pass filter. The presampled MTF accuracies of our method and the ESF-fitting method proposed by Boone and Seibert were compared by

use of different types of simulated ESFs as well as edge images from clinical CR and indirect-type flat panel detector (FPD) systems.

2 Materials and Methods

2.1 Simulated ESFs and edge images of clinical systems

2.1.1 Simulated ESFs without and with noise

First, a step-edge profile with 4096 data points and a data pitch of 0.02 mm was created. This step-edge profile was converted to ESFs without noise and with noise, which featured MTFs resembling a CR system and an indirect-type FPD system, respectively. These ESFs were assumed to have been obtained from edge images with a pixel pitch of 0.15 mm. The assumed photon number was $264,445 \text{ mm}^{-2}$, which corresponded to $2.58 \times 10^{-7} \text{ C/kg}$ (1.0 mR) at a radiation quality of RQA5 as described by an IEC standard (IEC 61267) [18], and therefore the pixel value for the direct exposure region was set to 5950, corresponding to a photon number of $0.15 \times 0.15 \text{ mm}^2$. As the exposure ratio of the opaque (tungsten) region to the direct exposure region was 0.25%, which was preliminarily measured on a CR system (Regius Model 210; Konica Minolta, Tokyo, Japan), for RQA5, the pixel value for the opaque region was set to 15. Thus, the noise-less step-edge profile had values of 5950 and 15 for the direct exposure and opaque sides, respectively, for simulating the data ratio between the two sides.

For generating another step-edge profile with noise, Poisson distribution noises with standard deviations equal to the square roots of the above mentioned pixel values (5950 and 15) were added to the direct exposure and opaque sides of the step-edge profile, respectively. In the presampled MTF analysis of actual edge images, the ESF noise was reduced through a binning process in which many reprojected pixels were averaged within each bin [8]. However, in the simulated ESF analysis used in this study, the noise-reduction effect of the binning process was not taken into account to examine more severe noise conditions than those encountered in actual images. Thus, we determined the severe noise levels from the square roots of the photon numbers on the direct exposure and opaque sides.

A one-dimensional Fourier transformation was applied to the edge profile, and a desired MTF was then multiplied in the frequency domain data. Finally, a 4096-point filtered edge profile with the desired MTF was generated through a one-dimensional inverse Fourier transformation. The two MTFs applied to the simulated ESFs, which resemble a CR system and an indirect-type FPD system, respectively, are shown in **Fig. 1**. The MTF for the indirect-type FPD had a LFD of approximately 9% to simulate the influence of glare. Consequently, four types of simulated edge profiles (CR-like ESFs without and with noise and FPD-like ESFs without and with noise) were obtained for the analysis. 10 ESFs were generated for each type of the simulated ESF with noise, and

they were used for statistical studies.

2.1.2 Clinical system edge images

a) CR images

A CR system (Regius Model 210; Konica Minolta, Tokyo, Japan) with a pixel pitch of 0.175 mm was employed. The edge image acquisition method was based on the recommendation made in the IEC 62220-1 [5]. A 1-mm-thick tungsten plate was imaged at a 200-cm source-to-detector distance (SDD) and an exposure dose at the detector surface of 2.58×10^{-7} C/kg (1 mR) with a beam quality of RQA5 [18].

b) Indirect-type FPD images

An indirect-type mammography FPD system (Senographe 2000D; GE Healthcare, Milwaukee, WI, USA) with a pixel pitch of 0.1 mm was employed. Image acquisition was performed based on a recommendation in the mammography-related IEC standard IEC 62220-1-2 [6]. The same tungsten plate used with the CR system was imaged using a 660-mm SDD and an exposure dose at the detector surface of 2.26×10^{-5} C/kg (87.5 mR) with the IEC-specified beam quality of RQA-M2 [18].

c) Direct-type FPD images

A direct-type mammography FPD system (Mammomat Inspiration; Siemens Healthcare, Erlangen, Germany) with a pixel pitch of 0.085 mm was employed. Similarly to the

indirect-type FPD, image acquisition was performed based on IEC 62220-1-2. The SDD was 650-mm, and an exposure dose at the detector surface was 6.05×10^{-5} C/kg (234 mR) with the beam quality of RQA-M2.

2.2 Edge data processing

2.2.1 Processing outline

The fundamental edge data processing used in our study was based on an established edge method [8]. Although, in this method, a Gaussian-weighted moving polynomial fit was applied to the ESF data for noise reduction, we excluded this process to compare the inherent noise-reduction performances of our proposed (variable filtering) method and the ESF-fitting method. **Figure 2** shows an outline of the procedures used for the presampled MTF analysis without noise reduction (non-processing method) as well as the variable filtering and ESF-fitting methods. Variable filtering was applied to LSF data obtained after the ESF differentiation process. ESF fitting was applied to the ESF data prior to the differentiation process. The simulated ESFs were processed from the differentiation process step while the linearization, reprojection, and binning steps were eliminated.

2.2.2 Non-processing method

For the CR image generated with use of the Regius Model 210, the pixel data were linearized based on the measured linear relationship between logarithm of exposure dose and pixel value for the RQA5 beam quality. For the FPD image generated by use of the Senographe 2000D, the exact linear relationship between the exposure dose and the pixel value was confirmed through a measurement using the RQA-M2 beam quality. Regions of interest (ROIs) that measured 512×128 pixels ($89.6 \times 22.4 \text{ mm}^2$) for CR and 1024×128 pixels ($102.4 \times 12.8 \text{ mm}^2$) for FPD, and contained the central part of the edge, were extracted from the respective edge images. The lengths of the ROI long axes were determined for correct measurement of the LFDs in the respective presampled MTFs [12, 16, 17]. The bin widths used in the binning process were set to 0.02 and 0.01 mm for the CR and FPD images, respectively. The resulting ESF data numbers for the CR and FPD images were 4096 and 8192, respectively.

2.2.3 Variable filtering method

The variable filtering method procedures were based on the non-processing method, and variable filtering was inserted after the ESF differentiation process.

Maintenance of the LSF tails is important for estimating the LFD accurately during the presampled MTF analysis [16]. Accordingly, the LSF tails correlate with the low-frequency region of the presampled MTF, and the region near the LSF center

inversely correlates with the high-frequency region. As shown in **Fig. 3**, when the frequency region below b is not filtered, the LSF tails outside of d are maintained and b can be calculated by $1/2d$. For example, for correctly estimating a low-frequency region at < 0.1 cycle/mm, the LSF tails outside of points at a ± 5.0 -mm distance from the LSF center should be measured accurately in a process that includes noise reduction. This means that a strong low-pass filter to cut off the frequency region > 0.1 cycle/mm can be applied to LSF tails beyond the ± 5.0 -mm points. Ideally, a low-pass filter with an extremely sharp edge at b is needed. However, this type of filter is known to cause ringing artifacts in the processed profiles. Therefore, we used Gaussian filters that did not cause ringing artifacts, accepting the slight MTF degradation caused by the filter response less than 1.0 at the boundary frequency b . To suppress the MTF degradation to the extent possible while obtaining effective noise reduction, the filter response at b was set to 0.97. This value was ascertained to provide an acceptable trade-off between the LSF noise-reduction effect beyond the points of $\pm d$ and the MTF maintenance in the frequency region below b . By using the filter response of 0.97, the maximum MTF degradation for above-mentioned simulated ESFs was constrained to be approximately 1.2% and 1.3% for CR-like and FPD-like ESFs, respectively ~~less than 1.5%~~ in frequency regions below the Nyquist frequencies. When the filter response of 0.95 was used, the maximum MTF degradation was approximately 2.0% and 2.2% for CR-like

and FPD-like ESFs, respectively. The filter response of 0.99 was inadequate due to its less noise reduction performance. The filter responses $FP(u, d)$, as a function of spatial frequency, u , and d , were determined as follows:

$$FP(u, d) = \exp\{-g(d)^2 u^2\}, \quad (1)$$

$$g(d) = 2d \sqrt{-\log_e 0.97}. \quad (2)$$

Figure 4 shows the filter examples at $d = 0.1, 0.5, 1.0,$ and 3.0 mm, and **Fig. 5** presents the variable filtering processing procedure for LSF data, $f(i)$ ($i = 0 \dots N-1$; N : LSF data number). First, the frequency components of LSF, $F(j)$ ($j = 0 \dots N-1$), were obtained through a discrete Fourier transformation. For d at data number i , d_i , the filtered frequency components $A(j, d_i)$ were calculated as $F(j) \times DFP(j, d_i)$ ($j = 0 \dots N-1$), after which an inverse discrete Fourier transformation was applied to obtain the filtered LSF for d_i , $a(k, d_i)$ ($k = 0 \dots N-1$). $DFP(j, d_i)$ denotes the filter responses corresponding to the data arrangement of discrete Fourier transformation result. The filtered LSF data, $f'(i)$, were assigned from $a(i, d_i)$. The above steps from the $DFP(j, d_i)$ multiplication to the $f'(i)$ assignment were repeated N times ($N = 4096$ for the simulated ESFs and CR images, and $N = 8192$ for the FPD images) to obtain the resultant filtered LSF. Any window functions prior to the Fourier transformation were not used, because the LSF tail values were sufficiently small ($< 10^{-5}$).

In variable filtering, as the distance between the point and the LSF center increases, a

stronger low-pass filter can be applied to the point. Therefore, the noise in the LSF tails can be effectively reduced. For the region near the LSF center, small values of $g(d)$, which form weak filters (or are nearly equal to no filter) can be used, thus maintaining the LSF shape in the region. As this variable filtering does not include a thresholding process, subjective adjustments are not needed for better noise reduction. The LSF center point used for determining d was calculated by averaging of the bisection positions between the points on both sides of the LSF at 40%, 50%, and 60% of the LSF peak.

2.2.4 ESF-fitting method

The ESF-fitting method procedures were based on those in the non-processing method and the ESF-fitting process was inserted after the projection and binning processes.

Boone and Seibert extended a study by Yin et al. [19] to perform an ESF-fitting process and subsequently proposed a fitting method in which an analytic equation represented the weighted sum of the exponential and error functions [15]. According to this method, we performed ESF-fitting by using the following equation:

if $x \geq 0$;

$$ESF_{fit}(x) = a_1 + a_2 \{1 - \exp(-a_3|x - a_4|)\} + a_5 \operatorname{erf}(a_6^{1/2}|x - a_4|), \quad (3)$$

if $x < 0$;

$$ESF_{fit}(x) = a_1 - a_2 \left\{ 1 - \exp(-a_3|x - a_4|) \right\} - a_5 \operatorname{erf}\left(a_6^{1/2}|x - a_4|\right), \quad (4)$$

where the six parameters, a_{1-6} , are fit coefficients and erf denotes the error function. A non-linear least-square technique was used for the fitting calculation, which combined the generalized reduced gradient algorithm and iterative calculations and was provided by the Solver add-in of the Excel spreadsheet application (Microsoft Corporation, Redmond, WA, USA). In the Solver add-in, the parameters of constraint precision and convergence were set to 10^{-6} and 10^{-4} , respectively.

2.3 Reproducibility of the determined MTF

The CR system, Regius Model 210, was used to investigate the reproducibility of the measured MTFs for the three ESF data processing methods. Ten edge images were obtained under the same image acquisition conditions, as described in Section 2.1.2, and the means and standard deviation values of the presampled MTFs for the 10 images were compared among the three methods. A one-way analysis of variance (ANOVA) followed by Tukey's test and the F-test were used for the statistical analyses of the mean and variance differences, respectively.

3 Results

3.1 Simulated ESF without noise

3.1.1 CR-like ESF

A comparison of the calculated MTFs of the variable filtering and ESF-fitting methods for the simulated CR-like ESF without noise and the true MTF is shown in **Fig. 6a**. **Figure 6b** presents the deviations between the true MTF and calculated MTFs as a function of spatial frequency. The calculated MTF of the variable filtering method was slightly lower than the true MTF. The ESF-fitting method provided a slightly larger deviation when compared with the variable filtering method. The maximum deviations of the variable filtering and ESF-fitting methods were 0.0027 and 0.0087, respectively.

3.1.2 FPD-like ESF

A comparison of the calculated MTFs of the variable filtering and ESF-fitting methods for the FPD-like ESF without noise and the true MTF is shown in **Fig. 7a**. **Figure 7b** presents the deviations between the true MTF and the calculated MTFs. The calculated MTF of the variable filtering method agreed precisely with the true MTF. In contrast, the ESF-fitting method failed the fitting and additionally could not reproduce the LFD in the MTF. The maximum deviation of the variable filtering method was 0.0077.

3.2 Simulated ESF with noise

3.2.1 CR-like ESF

Figures 8a and **b**, respectively, show the calculated MTFs and deviations from the true MTF of the three methods for the CR-like ESF with noise. Though we performed the MTF calculations using the 10 simulated ESFs for each method, a representative MTF curve, which indicated a reasonable deviation from the true MTF is presented in the figure. The MTF of the non-processing method oscillated severely around the true MTF. **Table 1** presents true MTF values and mean MTF values calculated from the 10 simulated ESFs using three methods. The values at 0.5, 1.0, 1.5, and 2.0 cycles/mm are indicated. The variable filtering and ESF-fitting methods disagreed slightly with the true MTF and the maximum deviations through the 10 simulated ESFs of these methods were 0.0181 and 0.0175, respectively.

3.2.2 FPD-like ESF

Figures 9a and **b**, respectively, show the calculated MTFs and deviations from the true MTF of the three methods for the FPD-like ESF with noise. Similarly to figure 8, the representative MTF curve for each method is presented in the figure. The MTF of the non-processing method also oscillated severely around the true MTF. Similar to the ESF without noise, the ESF-fitting method failed the fitting and was unable to reproduce the LFD in the MTF. **Table 2** presents true MTF values and mean MTF values calculated from the 10 simulated ESFs using the non-processing and variable filtering methods.

The variable filtering method exhibited excellent agreement with the true MTF, with a maximum deviation in 10 simulated ESFs of 0.0142.

3.3 Edge images from clinical systems

3.3.1 CR image

The measured, presampled MTFs of the three methods for the CR image are shown in **Fig. 10**. The presampled MTF of the non-processing method fluctuated because of noise in the LSF; severely oscillating MTF values were indicated, especially in the high spatial frequency region. The variable filtering method effectively suppressed these oscillations. The ESF-fitting method failed the fitting, even though the CR image appeared not to exhibit LFD in the presampled MTF. Therefore, the noise-reduction ability of the ESF-fitting method could not be evaluated.

3.3.2 Indirect-type FPD image

Figure 11 shows the measured, presampled MTFs of the three methods for the indirect-type FPD image. The presampled MTF of the non-processing method exhibited less fluctuation compared with the CR image. The variable filtering method also effectively suppressed these fluctuations. The ESF-fitting method failed the fitting in the frequency region above 0.2 cycle/mm, whereas the LFD in the frequency region below

0.2 cycle/mm was well fitted. Similar to the CR image, the noise elimination ability of the ESF-fitting method could not be evaluated because of the false fitting.

3.3.3 Direct-type FPD image

Figure 12 shows the measured, presampled MTFs of the three methods for the direct-type FPD image. The presampled MTF of the non-processing method exhibited fluctuations. The variable filtering method also effectively suppressed these fluctuations. The ESF-fitting method also failed the fitting, while the LFD in the frequency region below 0.07 cycle/mm was well fitted.

3.3.4 Reproducibility of the determined MTFs

Figure 13 shows comparisons of the mean presampled MTF values at 0.5, 1.0, and 2.0 cycles/mm in 10 CR images as measured using the three methods. Although the ESF-fitting method exhibited the highest reproducibility, this method failed the fitting for the 10 CR images, which is similar to the results displayed in **Fig. 10**. Therefore, this highest reproducibility was not of value to our evaluation. In addition, the mean values obtained with the ESF-fitting method differed significantly from those obtained with the non-processing and variable filtering methods at 0.5 and 1.0 cycle/mm ($P < 0.001$ for 0.5 and 1.0 cycle/mm; ANOVA and Tukey's test). The mean MTF values of the

non-processing and variable filtering methods were not significant ($P = 0.28, 0.20,$ and 0.93 for $0.5, 1.0,$ and 2.0 cycles/mm, respectively; ANOVA and Tukey's test), and the standard deviation values of the variable filtering method were significantly lower than those of the non-processing method ($P < 0.05$ for $0.5, 1.0,$ and 2.0 cycles/mm; F-test). Non-significant differences among the three methods were indicated at 2.0 cycles/mm, because the failed-fit curve obtained with the ESF-fitting method crossed the curves of the other two methods at a frequency near 2.0 cycles/mm.

4 Discussion

The variable filtering method provided improved filter performance, especially for LSF tails, because strong filters with very low cut-off frequencies could be applied to the LSF tails. However, we could not eliminate the effect of noise in the LSF. Therefore, we predicted that, if the ESF-fitting method could perform a successful fitting, it would be superior to the variable filtering method. In contrast to our prediction, the ESF-fitting method could not perform a successful fitting except for the simulated CR-like ESF. In the paper describing the ESF-fitting method [15], the author mentioned that the fitting coefficients in the method probably represent the longer range glare phenomenon characteristic in many imaging systems, implying insufficient robustness for absolute measurements of the glare fraction. However, the method failed the fittings of the

simulated FPD-like ESFs, for reproduction of not only the LFD (glare fraction) but also the entire MTF shape. The method also failed the fittings for all of the clinical systems we used (CR, indirect-type and direct-type FPDs), and only the LFDs in the indirect-type and direct-type FPDs' MTFs were correctly reproduced. Consequently, our results demonstrated a lower robustness of the ESF-fitting method; therefore, further improvement is sought for this method. However, because clinical systems have various presampled MTF shapes as indicated in our results, it may be difficult to develop a perfect fitting method that could be applied to all clinical systems.

In contrast, the variable filtering method was reasonably robust in terms of the two types of noisy simulated ESFs as well as the examined clinical CR, indirect-type FPD, and direct-type FPD system images. As the variable filter is basically a set of assembled Gaussian filters, it could not entirely eliminate the LSF noise. However, the filtering ability of this method became very strong, especially in the distant regions of the LSF tails, and thereby contributed to the remarkable suppression of MTF value fluctuations.

The slightly lower MTFs obtained with the variable filtering method for the CR- and FPD-like ESFs without noise (maximum deviations of 0.0027 and 0.0077 for CR- and FPD-like ESFs, respectively) resulted from a frequency response of 0.97 at the boundary frequency b . However, the noise-reduction effect necessarily decreased with an increase in the response value at b , and the lower the frequency response, the more

the presampled MTF was degraded. Given the uncertainty of the detective quantum efficiency (DQE) measurement, which has been recommended in IEC 62220-1 and 62220-1-2 (Δ DQE within ± 0.06 or Δ DQE/DQE within ± 0.1) [5, 6], the effect of the response value of 0.97 at b , as set in this study, could be determined to be sufficiently small. Therefore, the response value was reasonable for obtaining the presampled MTF, resulting in a less uncertain DQE measurement. For the simulated ESFs with noise, we set a much larger amount of noise than those observed in the clinical systems to examine the noise-reduction abilities of the proposed method. Although some fluctuations remained in the results, sufficient reduction ability was confirmed in terms of severe noise. The maximum deviations of 0.0181 for the 10 CR-like ESFs and 0.0142 for the 10 FPD-like ESFs in the noisy ESF results were also considered to be sufficiently small for the above-mentioned DQE uncertainty.

As a result, the variable filtering method exhibited sufficient noise-reduction effects and high reproducibility as compared with the non-processing method. Accordingly, the variable filtering method could contribute to reducing number of measurements for ESF averaging or MTF averaging, which has been needed to improve the presampled MTF accuracy.

Friedman and Cunningham proposed a method that incorporated open-field normalization, which allows the use of narrow ESFs (1-cm width) [16]. If this method

could be applied to detectors with glare, the enhanced noise in the LSF tail could be eliminated. However, the non-negligible errors indicated by the simulation results in that paper are problematic, and the effectiveness of this method has not been validated for various types of detectors.

Although we used only Gaussian filters for the variable filtering, other types of filters should be investigated in an attempt to increase the noise-reduction effect. One Fourier transformation and 4096 (8192 for Senographe 2000D) inverse Fourier transformation calculations with 4096 (8192 for Senographe 2000D) data points should be performed during variable filter processing. Although this computation load was somewhat heavy for a personal computer fitted with a Core i7 central processing unit (Intel Corporation, Santa Clara, CA, USA) and 3.1GHz clock frequency, the required computation time was not long (approximately 5 and 10 seconds for 4096 and 8192 data points, respectively).

5 Conclusion

We developed a variable filtering method for effectively reducing the LSF noise in presampled MTF measurements. This filter was comprised of Gaussian filters with position-dependent filter responses and enabled a strong LSF noise reduction. The excellent noise-reduction capability of this method was demonstrated by the results obtained for the simulated ESFs without and with noise and the edge images from the

clinical CR, indirect-type FPD, and direct-type FPD systems. We believe that this variable filtering method would improve the accuracy of presampled MTF measurements in DR systems.

COI statement

The authors declare that they have no conflict of interest.

References

1. Giger ML, Doi K. Investigation of basic imaging properties in digital radiography. I. Modulation transfer function. *Med Phys.* 1984;11:287-95.
2. Fujita H, Tsai DY, Itoh T, Doi K, Morishita J, Ueda K, Ohtsuka A. A simple method for determining the modulation transfer function in digital radiography. *IEEE Trans Med Imaging.* 1992;11:34-9.
3. Fujita H, Ueda K, Morishita J, Fujikawa T, Ohtsuka A, Sai T. Basic imaging properties of a computed radiographic system with photostimulable phosphors. *Med Phys.* 1989;16:52-9.
4. Fujita H, Doi K, Giger ML. Investigation of basic imaging properties in digital radiography. 6. MTFs of II-TV digital imaging systems. *Med Phys.* 1985;12:713-20.

5. IEC 62220-1. Medical electrical equipment - Characteristics of digital X-ray imaging devices - Part 1: Determination of the detective quantum efficiency, ed. 1.0, 2003.
6. IEC 62220-1-2. Medical electrical equipment - Characteristics of digital X-ray imaging devices - Part 1-2: Determination of the detective quantum efficiency - Detectors used in mammography, ed. 1.0, 2007.
7. Buhr E, Günther-Kohfahl S, Neitzel U. Accuracy of a simple method for deriving the presampled modulation transfer function of a digital radiographic system from an edge image. *Med Phys.* 2003;30:2323-31.
8. Samei E, Flynn MJ, Reimann DA. A method for measuring the presampled MTF of digital radiographic systems using an edge test device. *Med Phys.* 1998;25:102-13.
9. Greer PB, van Doorn T. Evaluation of an algorithm for the assessment of the MTF using an edge method. *Med Phys.* 2000;27:2048-59.
10. Cunningham IA, Reid BK. Signal and noise in modulation transfer function determinations using the slit, wire, and edge techniques. *Med Phys.* 1992;19:1037-44.
11. Cunningham IA, Fenster A. A method for modulation transfer function determination from edge profiles with correction for finite-element differentiation. *Med Phys.* 1987;14:533-7.
12. Samei E, Ranger NT, Dobbins JT 3rd, Chen Y. Intercomparison of methods for image quality characterization. I. Modulation transfer function. *Med Phys.*

2006;33:1454-65.

13. Donovan M, Zhang D, Liu H. Step by step analysis toward optimal MTF algorithm using an edge test device. *J Xray Sci Technol.* 2009;17:1-15.

14. Neitzel U, Günther-Kohfahl S, Borasi G, Samei E. Determination of the detective quantum efficiency of a digital x-ray detector: comparison of three evaluations using a common image data set. *Med Phys.* 2004;31:2205-11.

15. Boone JM, Seibert JA. An analytical edge spread function model for computer fitting and subsequent calculation of the LSF and MTF. *Med Phys.* 1994;21:1541-5.

16. Friedman SN, Cunningham IA. Normalization of the modulation transfer function: the open-field approach. *Med Phys.* 2008;35:4443-9.

17. Carton AK, Vandenbroucke D, Struye L, Maidment AD, Kao YH, Albert M, Bosmans H, Marchal G. Validation of MTF measurement for digital mammography quality control. *Med Phys.* 2005;32:1684-95.

18. IEC 61267. Medical diagnostic X-ray equipment - Radiation conditions for use in the determination of characteristics, ed. 2.0, 2005.

19. Yin FF, Giger ML, Doi K. Measurement of the presampling modulation transfer function of film digitizers using a curve fitting technique. *Med Phys.* 1990;17:962-6.

Fig. 1 Set MTFs for simulated ESFs, resembling CR and indirect-type FPD systems

Fig. 2 Presampled MTF data analysis processing steps for the non-processing, variable filtering, and ESF-fitting methods

Fig. 3 Relationship between the boundary frequency b in the presampled MTF and distance d in the LSF. The LSF tails outside of d are maintained when the frequency region below $b (= 1/2d)$ is not filtered

Fig. 4 Filter examples at $d = 0.1, 0.5, 1.0,$ and 3.0 mm, used in the variable filter

Fig. 5 Variable filtering processing procedure

Fig. 6 a True and calculated presampled MTFs of the variable filtering and ESF-fitting methods for a simulated CR-like ESF without noise; **b** deviations from the true MTFs as a function of spatial frequency

Fig. 7 a True and calculated presampled MTFs of the variable filtering and ESF-fitting methods for a simulated FPD-like ESF without noise; **b** deviations from the true MTFs as a function of spatial frequency

Fig. 8 a True and calculated presampled MTFs generated with the non-processing, variable filtering, and ESF-fitting methods used for a simulated CR-like ESF with noise; **b** deviations from the true MTFs as a function of spatial frequency

Fig. 9 a True and calculated presampled MTFs generated with the non-processing, variable filtering, and ESF-fitting methods used for a simulated FPD-like ESF with

noise; **b** deviations from the true MTFs as a function of spatial frequency

Fig. 10 Presampled MTFs from a clinical CR system, calculated with the three methods

Fig. 11 Presampled MTFs from a clinical indirect-type FPD system, calculated with the three methods

Fig. 12 Presampled MTFs from a clinical direct-type FPD system, calculated with the three methods

Fig. 13 Comparisons of mean presampled MTF values at **a** 0.5 cycle/mm, **b** 1.0 cycle/mm, and **c** 2.0 cycles/mm, measured in 10 CR images with the three methods

Table 1 True MTF values and mean MTF values with standard deviations calculated using three methods for ten simulated noisy CR-like ESFs

Table 2 True MTF values and mean MTF values with standard deviations calculated using three methods for ten simulated noisy FPD-like ESFs. Values of the ESF-fitting method are not presented because the method failed the fitting for all of the ESFs

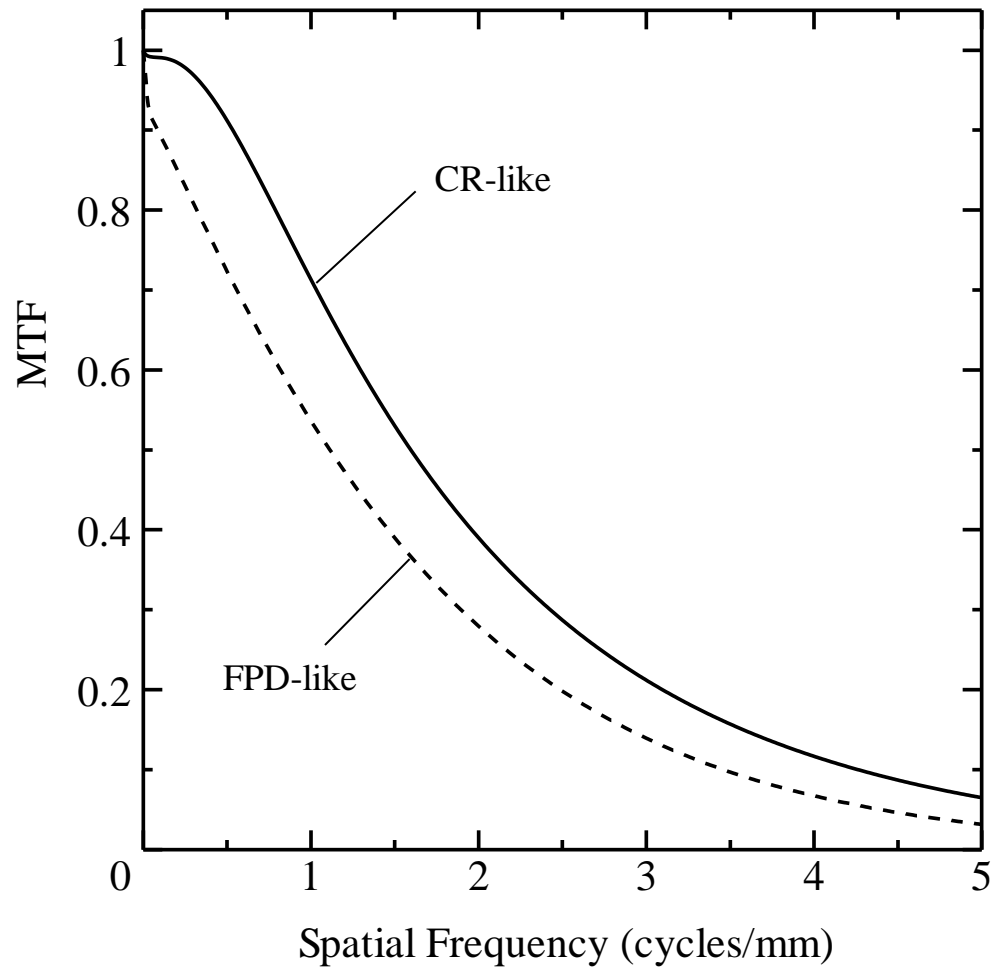
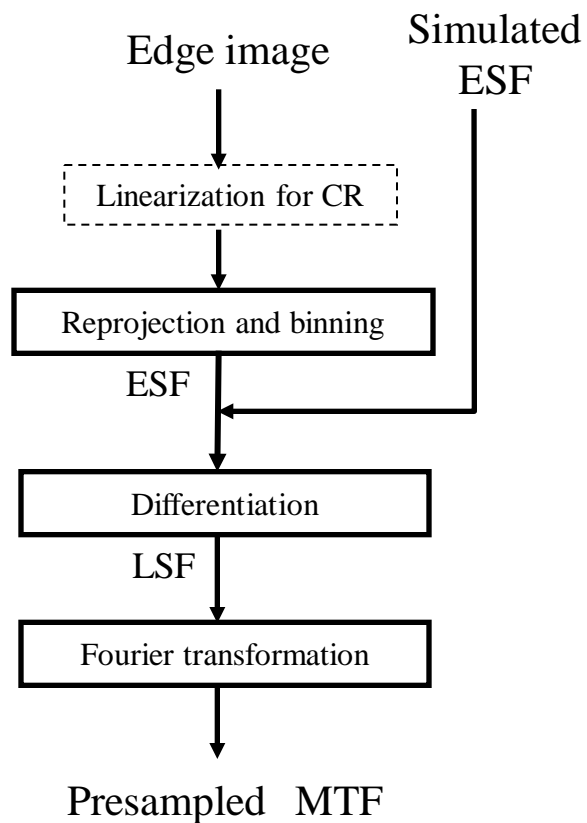
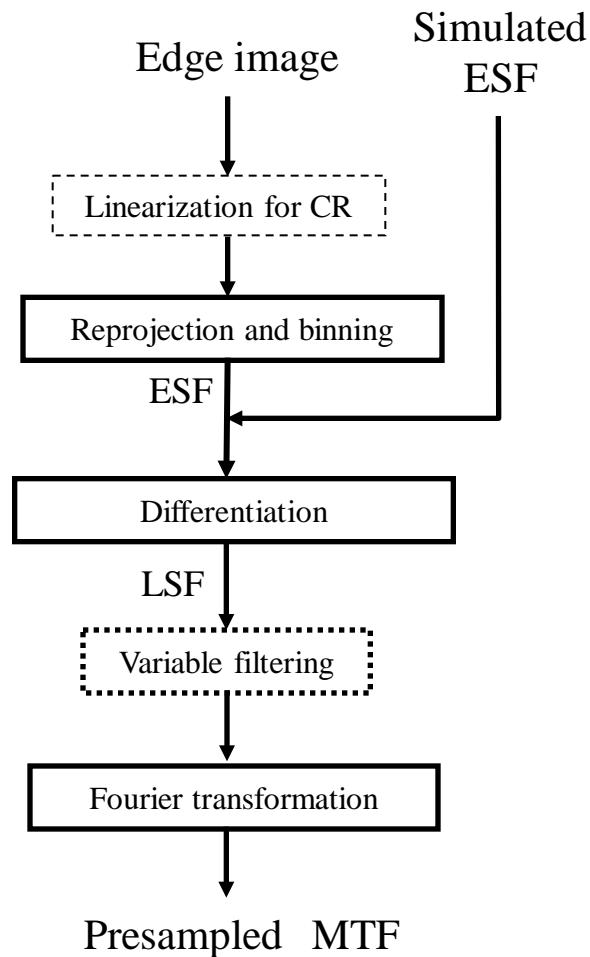


Fig. 1 Set MTFs for simulated ESFs, resembling CR and indirect-type FPD systems

Non-processing method



Variable filtering method



ESF-fitting method

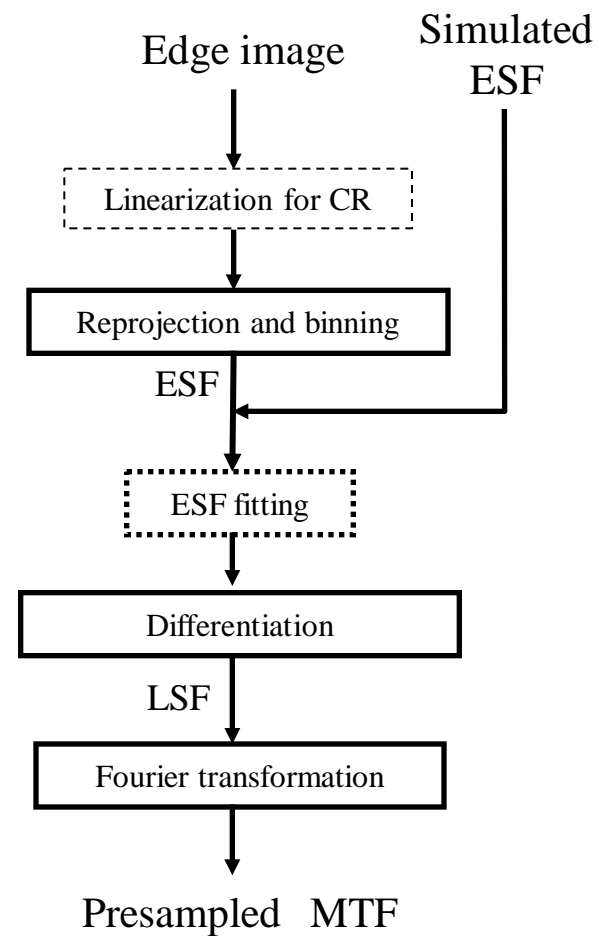


Fig. 2 Presampled MTF data analysis processing steps for the non-processing, variable filtering, and ESF-fitting methods

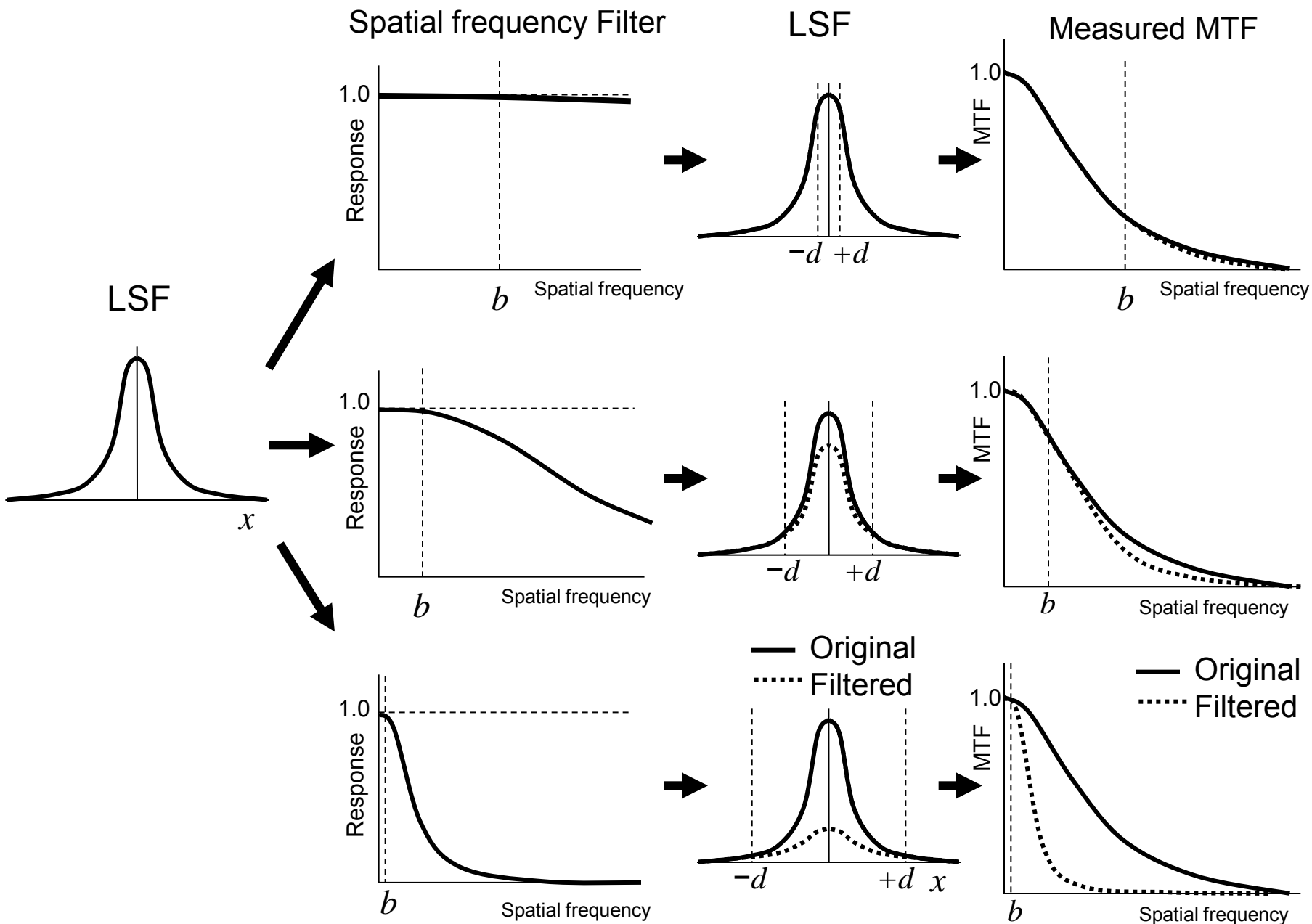


Fig. 3 Relationship between the boundary frequency b in the presampled MTF and distance d in the LSF. The LSF tails outside of d are maintained when the frequency region below $b (= 1/2d)$ is not filtered

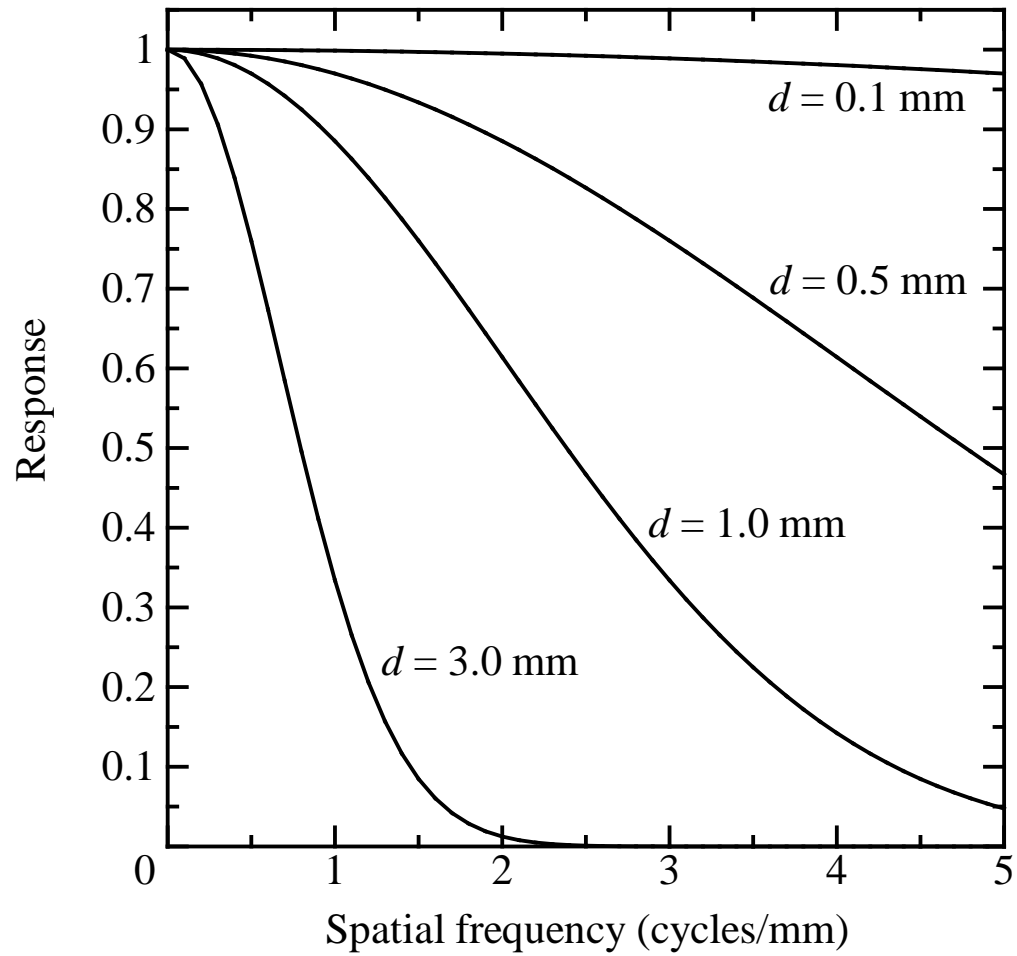


Fig. 4 Filter examples at $d = 0.1, 0.5, 1.0,$ and 3.0 mm, used in the variable filter

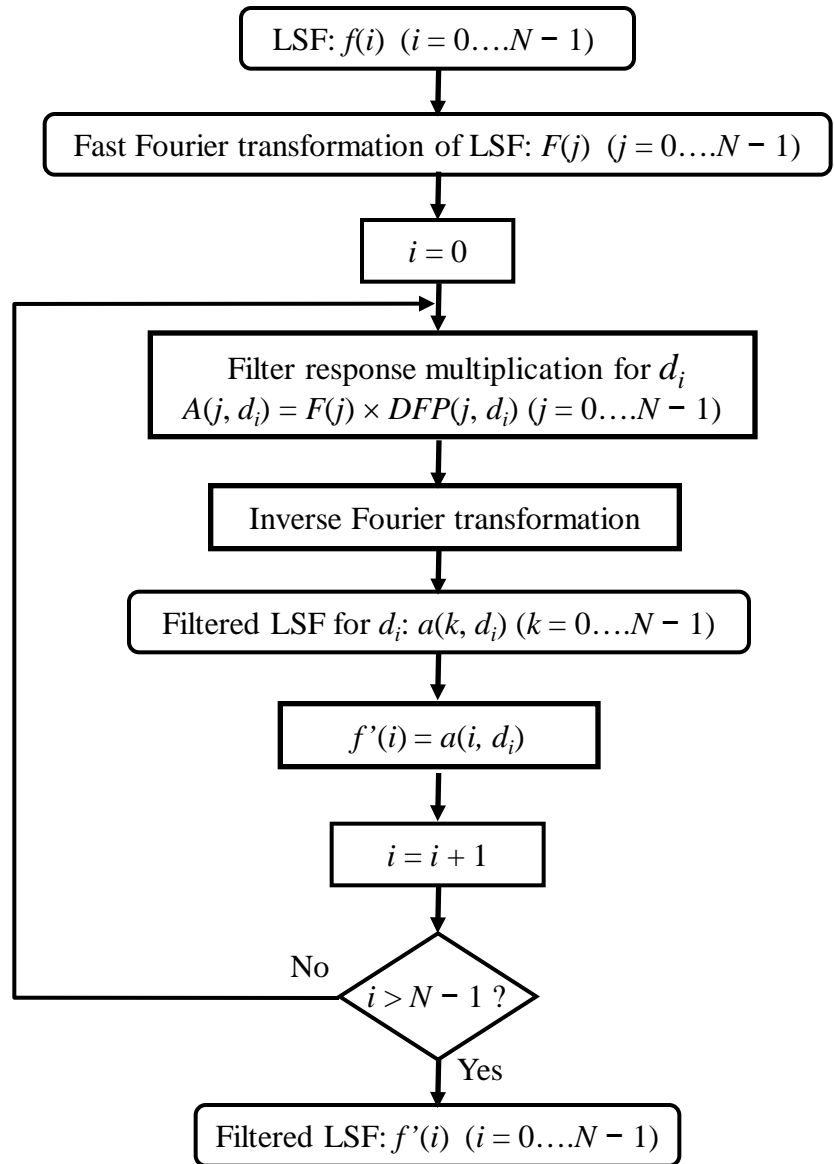
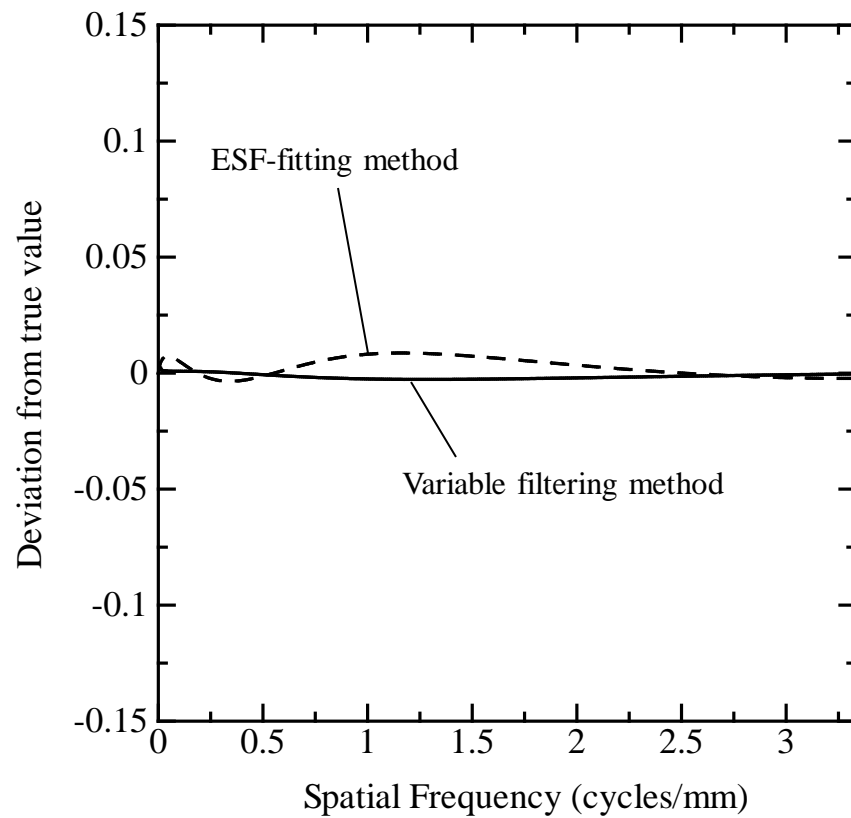
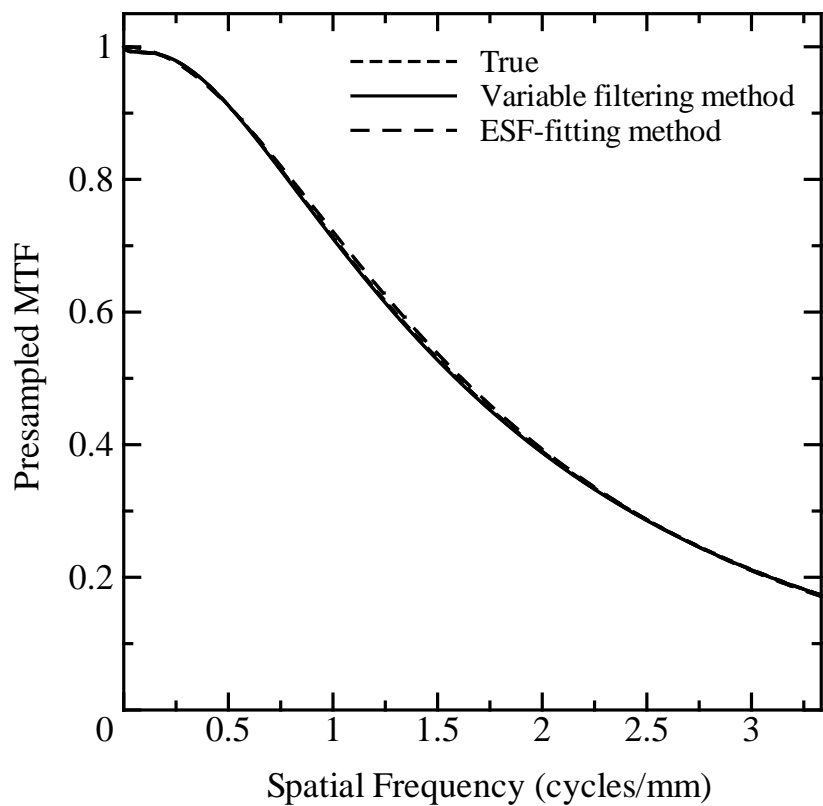
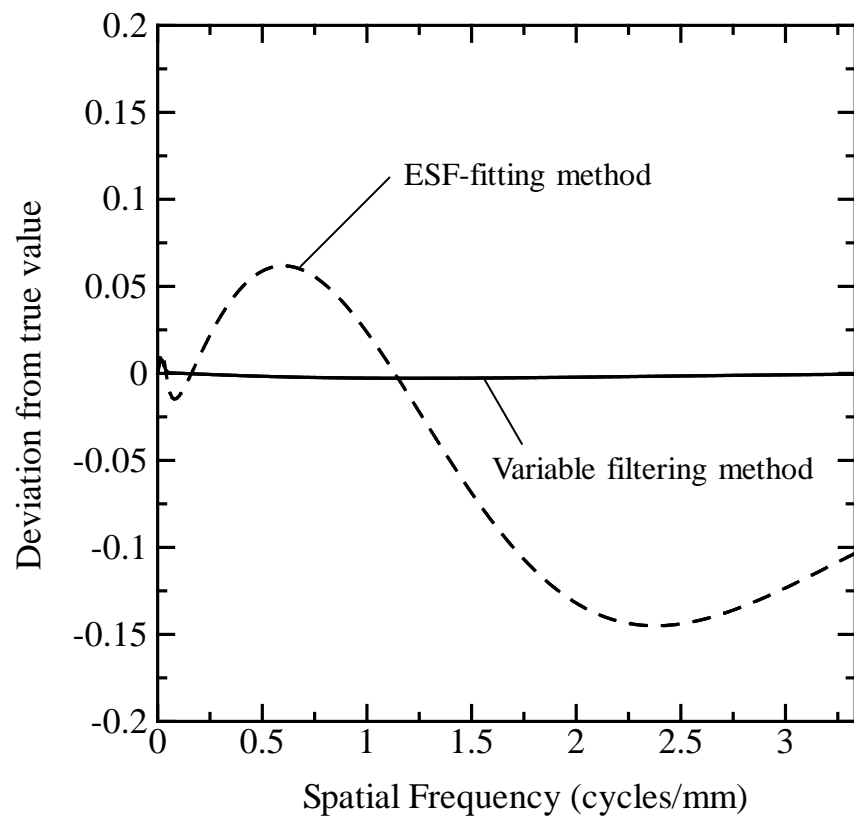
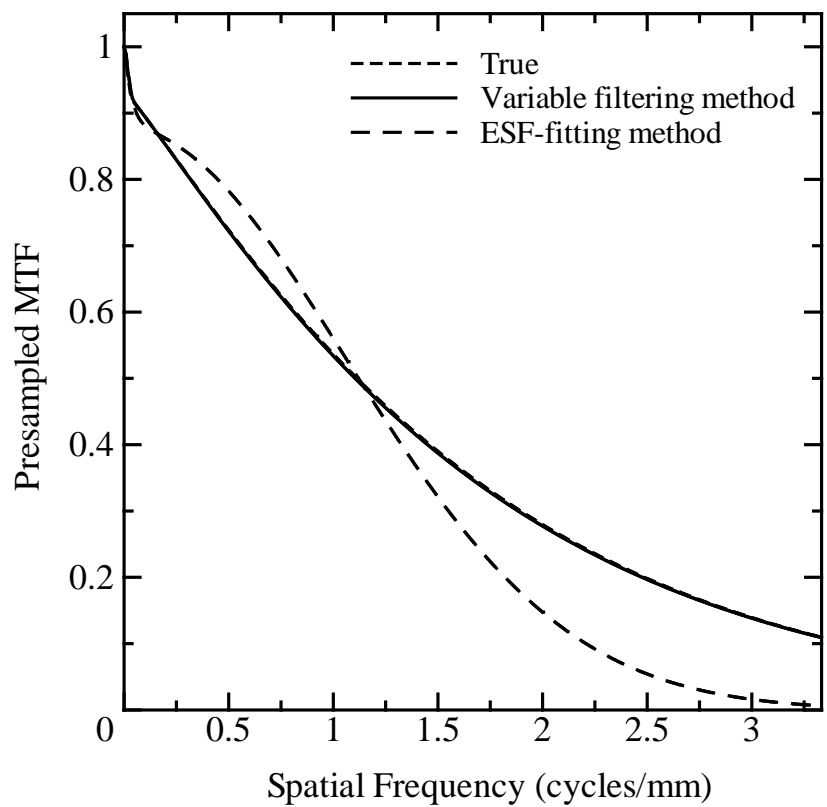


Fig. 5 Variable filtering processing procedure



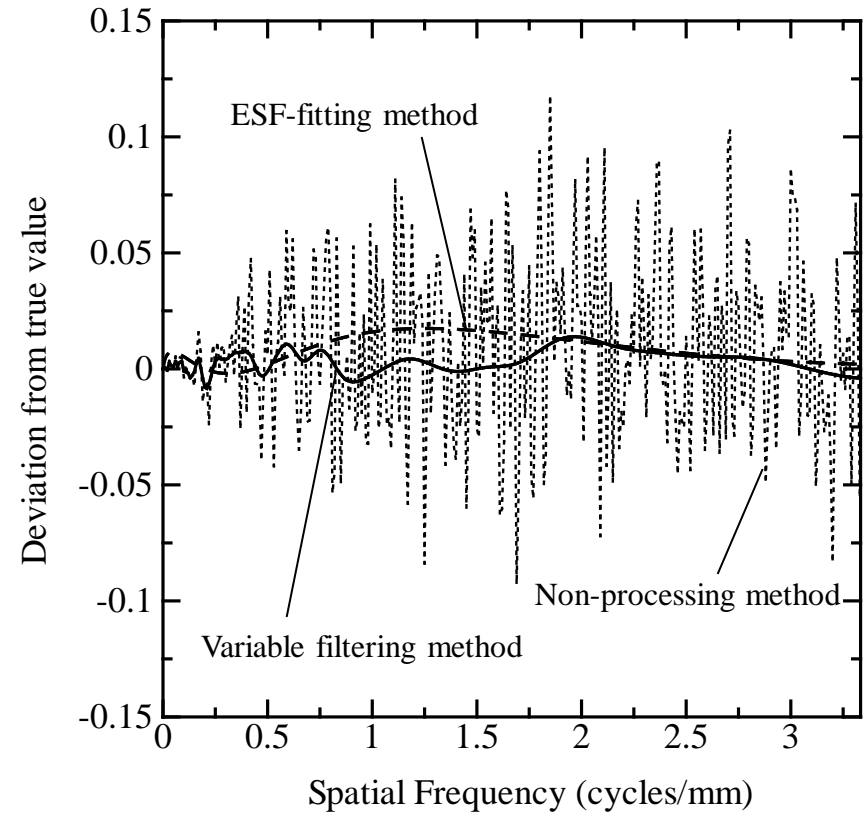
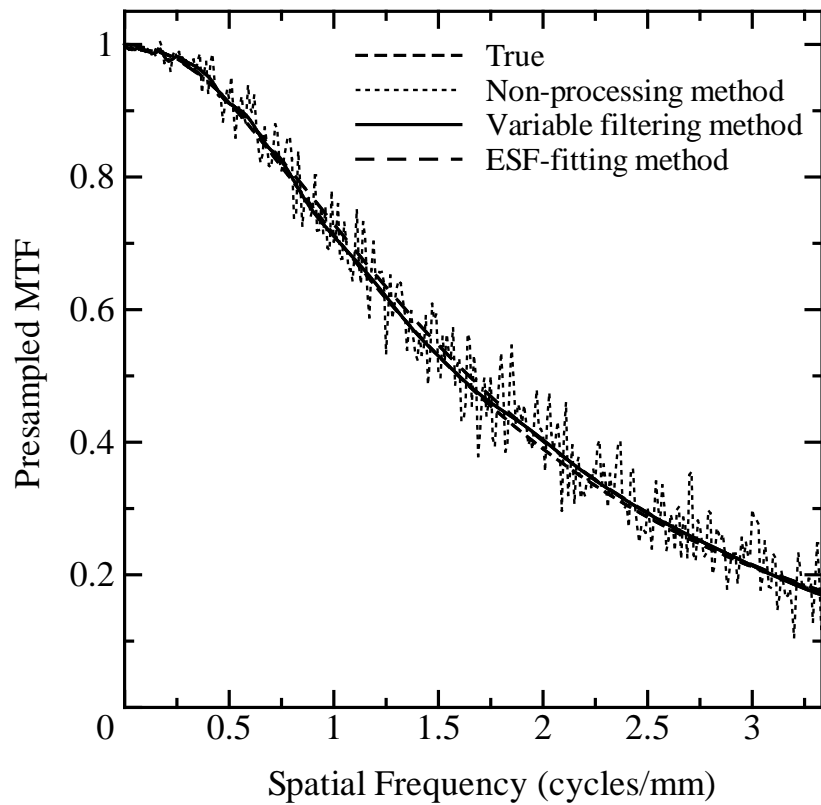
a | b

Fig. 6 a True and calculated presampled MTFs of the variable filtering and ESF-fitting methods for a simulated CR-like ESF without noise; **b** deviations from the true MTFs as a function of spatial frequency



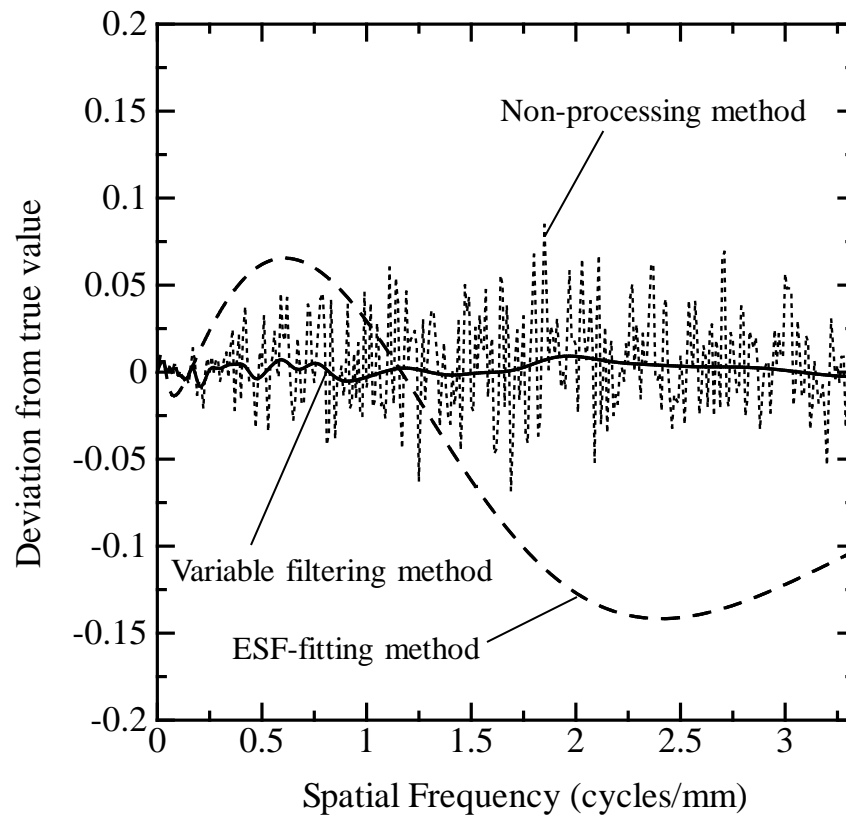
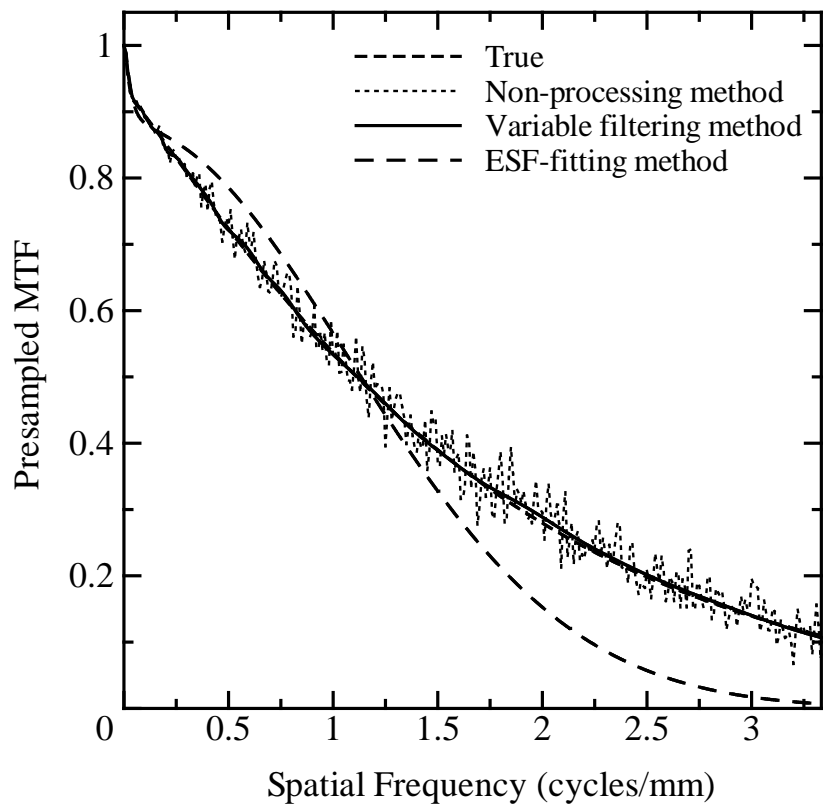
a | b

Fig. 7 a True and calculated presampled MTFs of the variable filtering and ESF-fitting methods for a simulated FPD-like ESF without noise; **b** deviations from the true MTFs as a function of spatial frequency



a | b

Fig. 8 **a** True and calculated presampled MTFs generated with the non-processing, variable filtering, and ESF-fitting methods used for a simulated CR-like ESF with noise; **b** deviations from the true MTFs as a function of spatial frequency



a | b

Fig. 9 a True and calculated presampled MTFs generated with the non-processing, variable filtering, and ESF-fitting methods used for a simulated FPD-like ESF with noise; **b** deviations from the true MTFs as a function of spatial frequency

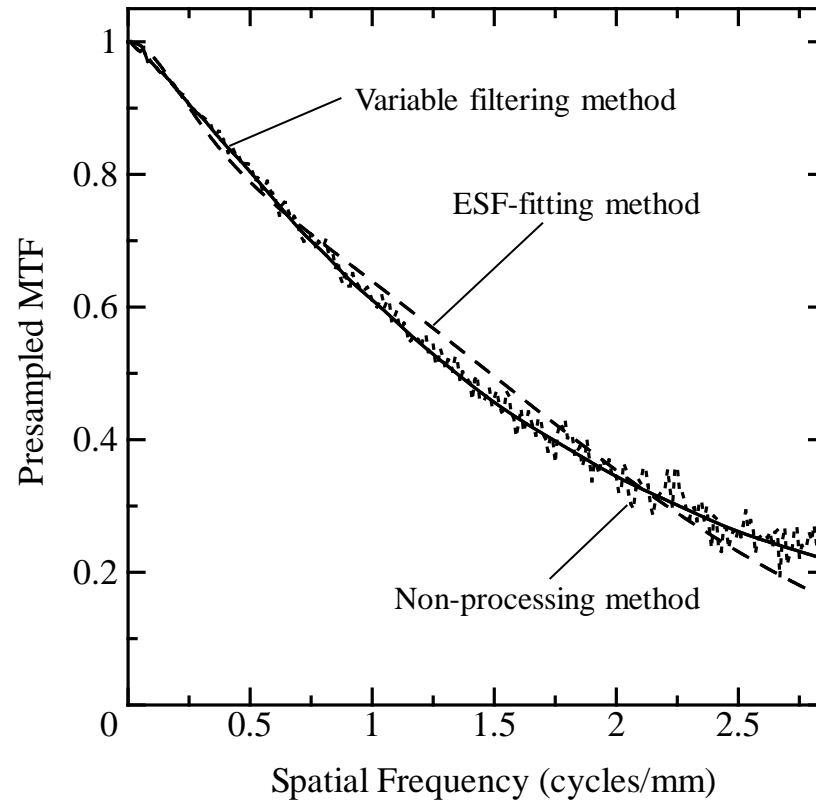


Fig. 10 Presampled MTFs from a clinical CR system, calculated with the three methods

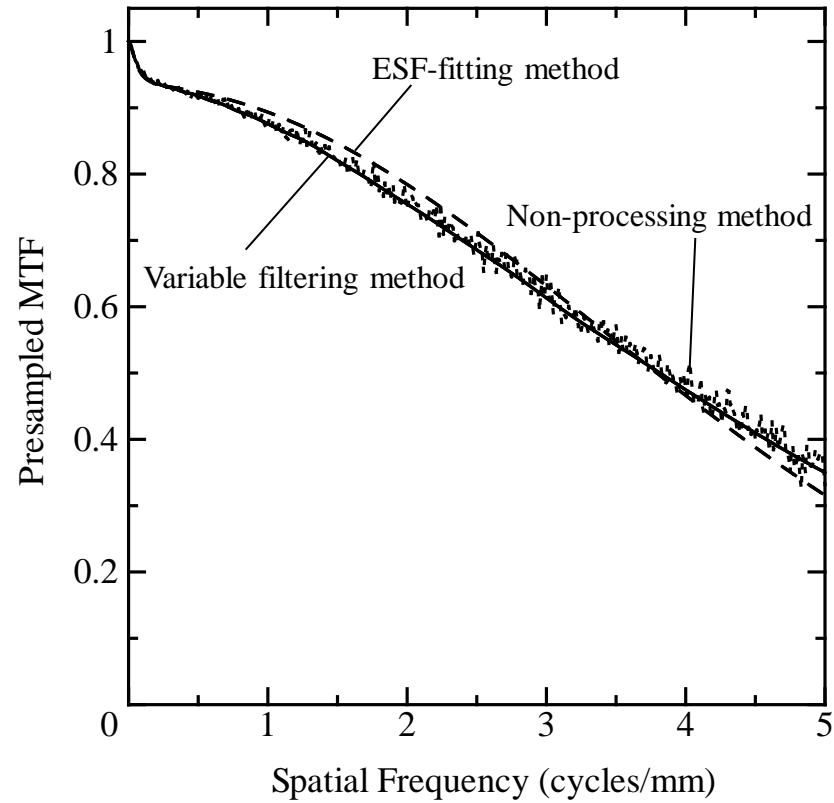


Fig. 11 Presampled MTFs from a clinical indirect-type FPD system, calculated with the three methods

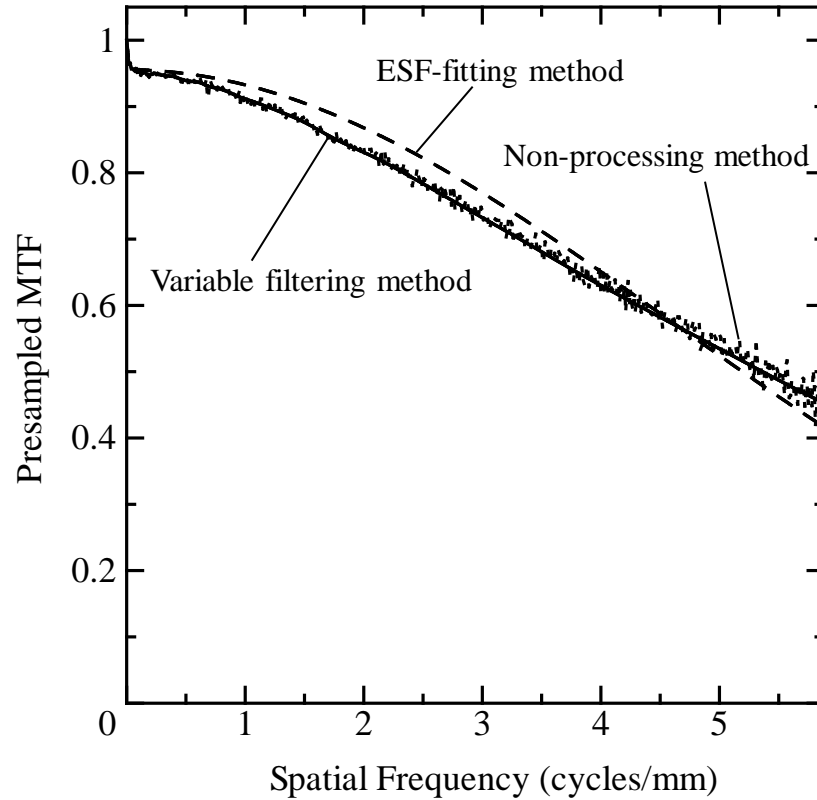
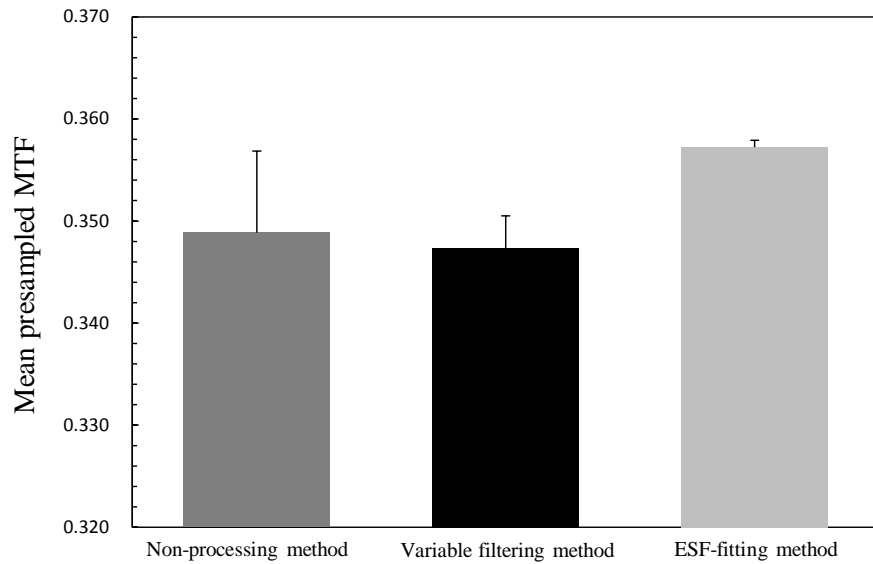
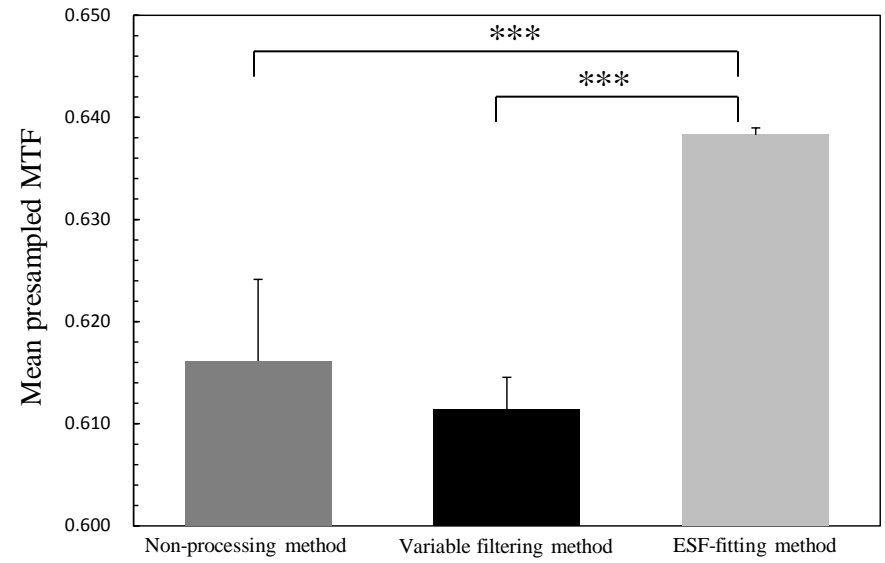
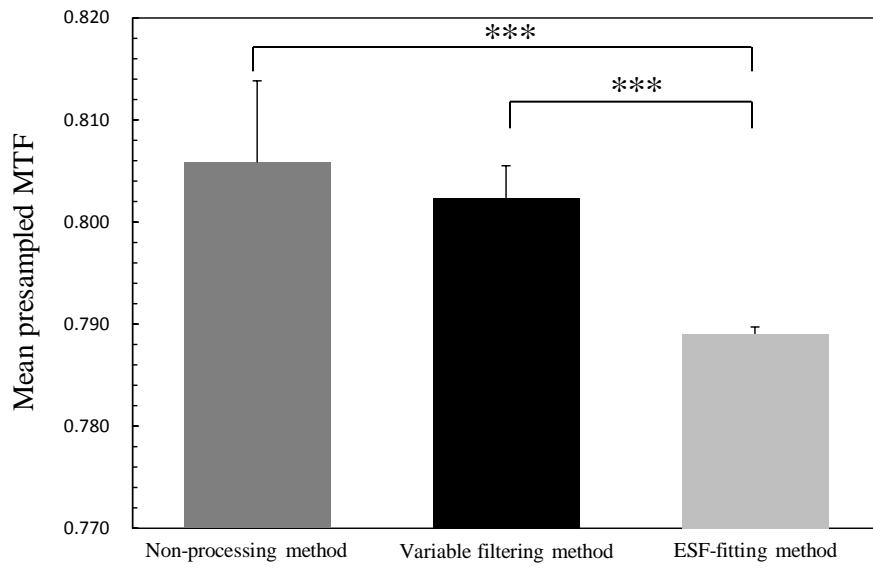


Fig. 12 Presampled MTFs from a clinical direct-type FPD system, calculated with the three methods



*** $P < 0.001$

a	b
c	

Fig. 13 Comparisons of mean presampled MTF values at **a** 0.5 cycle/mm, **b** 1.0 cycle/mm, and **c** 2.0 cycles/mm, measured in 10 CR images with the three methods

	0.5 cycle/mm	1.0 cycle/mm	1.5 cycles/mm	2.0 cycles/mm
True	0.912	0.713	0.530	0.390
Non-processing method	0.917 (0.019)	0.712 (0.049)	0.539 (0.064)	0.399 (0.051)
Variable filtering method	0.910 (0.005)	0.709 (0.010)	0.527 (0.004)	0.388 (0.008)
ESF-fitting method	0.911 (0.002)	0.722 (0.005)	0.538 (0.005)	0.393 (0.004)

Note: Data for three methods are mean MTF values, and data in parentheses are standard deviations.

Table 1 True MTF values and mean MTF values with standard deviations calculated using three methods for ten simulated noisy CR-like ESFs

	0.5 cycle/mm	1.0 cycle/mm	1.5 cycles/mm	2.0 cycles/mm
True	0.724	0.537	0.390	0.280
Non-processing method	0.727 (0.016)	0.535 (0.037)	0.396 (0.047)	0.286 (0.036)
Variable filtering method	0.721 (0.004)	0.533 (0.007)	0.387 (0.003)	0.277 (0.006)

Note: Data for three methods are mean MTF values, and data in parentheses are standard deviations.

Table 2 True MTF values and mean MTF values with standard deviations calculated using three methods for ten simulated noisy FPD-like ESFs. Values of the ESF-fitting method are not presented because the method failed the fitting for all of the ESFs